Chemical potential of inhomogeneous single-layer graphene

E. M. Hajaj,[1,2] O. Shtempluk,[2] V. Kochetkov,[2] A. Razin,[2] and Y. E. Yaish[2]

[1]*Russell Berrie Nanotechnology Institute, Technion, Haifa, Israel 32000*

[2]*Department of Electrical Engineering, Technion, Haifa, Israel 32000*

In this paper, we present measurements of the chemical potential of single-layer graphene as a function of carrier density and temperature, including near the Dirac point. Far from the charge neutrality point, the graphene is homogenous with a single carrier type. However, as the Dirac point is approached, puddles form, and electrons and holes coexist. Hall effect analyses based on two charge carriers are not adequate in this regime. Hence, a new methodology is introduced, and by using the chemical potential and the transport data self-consistently, we were able to extract the density of each carrier. We obtained very good agreement with a recent theory that assumes a Gaussian distribution of the electrostatic disorder potential. Surprisingly, the temperature dependence of the minimum conductivity of graphene was primarily attributed to the temperature dependence of the disorder potential itself through the carrier charge densities, and not to the temperature dependence of the carrier's mobility.
.

PACS number(s): 72.80.Vp

I. INTRODUCTION

Many of the unique electrical properties of single-layer graphene (SLG) have been attributed to the linear dispersion relation and to the linear density of states (DOS) of the zero band gap of graphene. Several experiments conducted on SLG found the predicted noninteracting DOS with a small correction to the inverse compressibility of graphene due to the electron-electron interaction.[1–7] In most of these studies, the primary technique is based on measuring the change in the graphene chemical potential, $\delta\mu$, under periodic modulation of the gate bias, δV_g, which is responsible for the change in the hole carrier density, δp, for example. Because the DOS, and the compressibility, are given by $\frac{\partial p}{\partial \mu}$, δp is usually extracted from either the gate bias or the Hall data. However, as the system is tuned towards the Dirac point, the graphene charge carriers break into puddles, where electrons (n) and holes (p) coexist. Moreover, because μ is not a linear function of the carrier density, the gate bias induces unequal changes in the electron and hole densities. Consequently, for those experiments that directly measure the quantum capacitance, which is proportional to the compressibility, the density assignment is inadequate in the nonhomogeneous regime. Thus, these two obstacles may lead to inaccurate estimates of the electron-electron exchange and correlation contributions, which are of significant physical importance because of their many-body origin.

A common method for the extraction of the densities of p and n is based on the two-band model for the Hall effect.[8] However, in the inhomogeneous regime, this method is inadequate because this model for the Hall effect was derived for situations in which these two carriers share the same region in space. However, this is not the case for graphene. Although electrons and holes coexist near the charge neutrality point (CNP), at zero temperature they never share the same region in space. As will become evident later in this study, the disorder potential strength is $\approx$100 meV; thus even at room temperature, our assumptions that the fraction of minority carriers is negligible in the same puddle as the majority carrier is well justified. Clear evidence for incorrect

carrier values predicted by the Hall model can be found at the Dirac point itself. According to Eq. (1), where σ and R_h are the conductivity and Hall resistance, respectively, and μ_n and μ_p are the electron and hole mobilities, at the CNP, $n_H = p_H \simeq \sigma/2e\mu_0$, where e is the absolute electron charge, and it was assumed that $\mu_0 = \mu_p = \mu_n$, as is typically the case. However, from the usual expression for the conductivity, at the Dirac point we obtain $n_D = p_D = \sigma/e\mu_0$, where n_D (p_D) is the average electron (hole) density in the electron (hole) puddles only. Thus, the extracted densities from Eq. (1) are half of the correct values. The reason is obvious. Because the two-carrier-type Hall model assumes spatial coexistence of the charges in the entire sample, the carrier density of the two-carrier model should be half of the correct density to fulfill the conductivity equation.

$$p_H = \frac{\sigma(\mu_n + R_h\sigma)}{e\mu_p(\mu_n + \mu_p)}, \quad n_H = \frac{\sigma(\mu_p - R_h\sigma)}{e\mu_n(\mu_n + \mu_p)}. \quad (1)$$

The lack of accurate measurements of the carrier densities for the inhomogeneous regime causes severe problems not only for the DOS and the compressibility measurements, from which the electron-electron interactions can be derived, but also for understanding transport behavior in this regime. There are several mean-field theories that predict electrical conductance at the Dirac point, but most of these theories are based on residual doping, which ignores differences between the carrier types. Knowing the correct densities can shed light on the temperature and magnetic field dependence of graphene conductance in the inhomogeneous regime.

Alternatively, it is possible to measure the chemical potential, and to derive from it the inverse compressibility and the DOS. For gated, p-type graphene far from the CNP, the relation between the external voltage and the chemical potential is given by

$$V_g = \frac{ep}{c_g} + \mu(p)/e + \phi_0, \quad (2)$$

where c_g is the geometric gate-graphene capacitance per unit area, and ϕ_0 is the electrical potential attributed to residual doping. Usually, the geometric capacitance is much
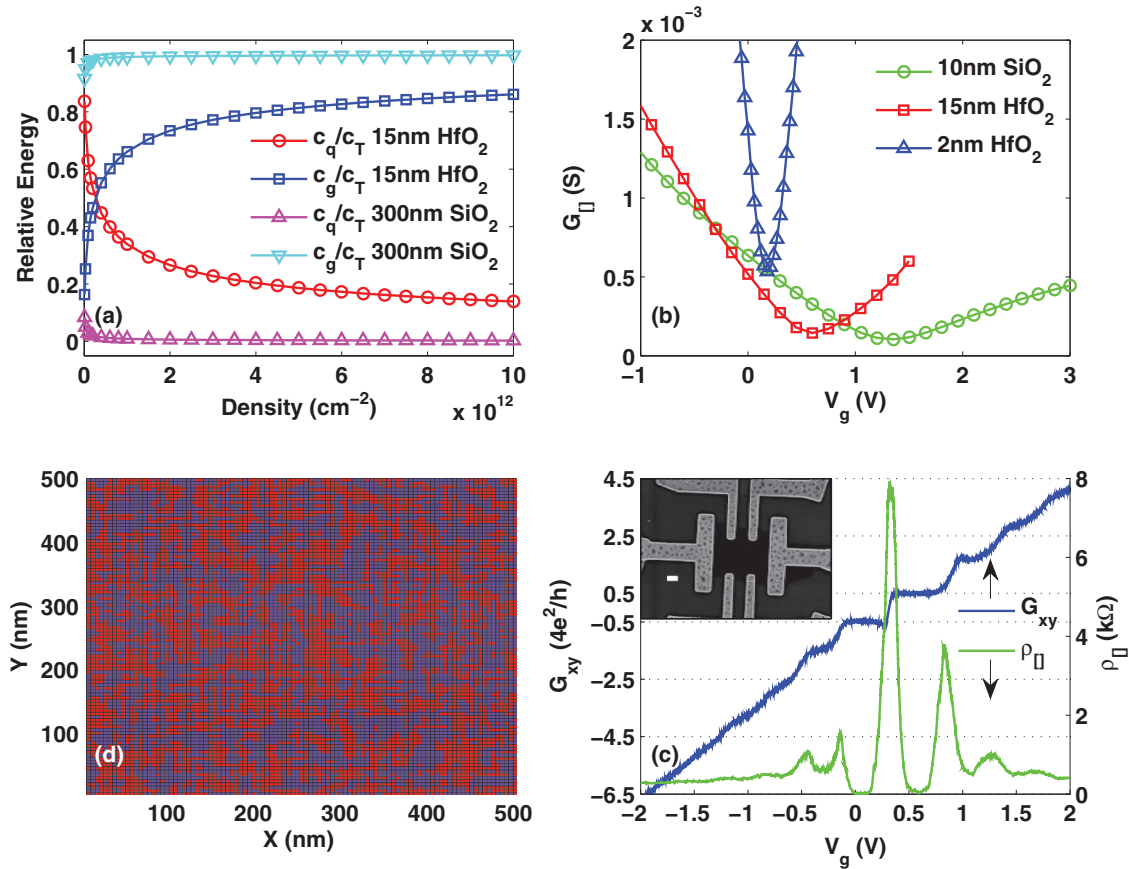
FIG. 1. (Color online) (a) Relative energy contribution with respect to carrier density according to Eq. (1), calculated at zero temperature and $\phi_0 = 0$. Light blue and blue (down triangle and square) indicate the geometrical term for gate oxides of 300 nm of SiO_2 and 15 nm of HfO_2, respectively, and magenta and red (triangle and circle) indicate the quantum contributions for gate oxides of 300 nm of SiO_2 and 15 nm of HfO_2, respectively. (b) Sheet conductance ($G_\square$) as a function of gate voltage for three different substrates. (c) Quantum Hall measurement for SLG on 15 nm of HfO_2 at $T = 1.7$ K and a magnetic field $B = 8.5$ T. Blue and green lines are G_{xy} and $\rho_\square$, respectively. Inset: Typical scanning electron microscopy (SEM) image of an SLG device on HfO_2. The scale bar is 2 μm. (d) Spatial distribution of electron (blue) and hole (red) puddles based on the Gaussian disorder distribution [Eq. (7)], with $s = 100$ meV.

smaller than the quantum capacitance, $c_q = e^2 \frac{\partial p}{\partial \mu}$, and the chemical potential is a small contribution to Eq. (2); this small contribution makes measurements of the DOS challenging. However, if one dramatically increases c_g, either by using a thinner oxide layer, using a high dielectric material, or using both, the quantum term will no longer be negligible. In Fig. 1(a), we depict the relative contributions of the geometric and quantum terms with respect to the total energy (eV_g) as a function of the carrier density, for two extreme cases. The first case, plotted in light blue (c_g) and magenta (c_q), reflects the relative contributions for a 300 nm SiO_2 gate oxide in which the quantum part is negligible. The second case (blue and red) shows the same two relative contributions for 15 nm of HfO_2, which was one of the gate oxides that we used in this study, with a dielectric constant of $\epsilon = 15$. Clearly, one can see that for densities below 10^{12} cm^{-2} the quantum term is more than 30% of the total energy, and drops slowly to ~15% as the density increases to 10^{13} cm^{-2}.

II. EXPERIMENTAL

In this study we prepare several types of devices, all composed of single-layer graphene (SLG) on top of highly

p-doped silicon substrates with a thin oxide layer of 2 or 15 nm HfO_2, 10 nm SiO_2, and 50 and 100 nm Si_3N_4. The fabrication process is described elsewhere,[9] and a typical scanning electron microscopy (SEM) image of a complete device with Hall bar shape, and the transfer characteristics are presented in Figs. 1(b) and 1(c). Many of these devices have high transconductance ($g_m = \partial I/\partial V_g/W$, where W is the device width), and the highest g_m we have measured at room temperature and under ambient conditions was 700 μS/μm at $V_{DS} = 1$ V. After subtracting the contact resistance of the device, one finds $g_m \simeq 11$ mS/μm, which is the highest transconductance ever measured for SLG to the best of our knowledge (see Fig. 1S in the Supplemental Material[10]). The normalized g_m, which takes into account the geometrical dimensions of the device and the bias voltage at which the measurements were performed, is given by $g_{mN} = Lg_m/V_{DS} = \mu c_g$[11] and was found to be 2.8 (44) mF V^{-1} s^{-1} with (without) contact resistance. From direct measurements of the mobility, using the Hall effect, one obtains $c_g = 1.6 \pm 0.1$ μF cm^{-2}, which is in good agreement with the expected theoretical value of 1.7 μF cm^{-2}. This gate capacitance is 130 times larger than that of the usual 285 nm SiO_2 based capacitor, and is the largest capacitance published to date.

With quantum Hall effect measurements, we verified that all of the devices we present in this study consist of SLG [see Fig. 1(c)]. The measurements were performed at various temperatures from 1.5 K to 300 K under vacuum with a lock-in technique and low bias excitation. They included two- and four-probe measurements of the longitudinal and the transverse voltages and the total current through the device. The mobility was calculated at high densities ($>5 \times 10^{12}$ cm^{-2}) and was found to be in the range of 1000–15 000 cm^2 V^{-1} s^{-1} prior to annealing. After annealing with high current at 300 K in vacuum, the mobility increased by approximately a factor of two to 30 000 cm^2 V^{-1} s^{-1}.[12,13] These somewhat moderate mobilities are because of the ∼1 nm thin layer of polymethylmethacrylate (PMMA) that remains underneath the SLG at the end of the fabrication process. For homogenous graphene, the carrier density was measured by the Hall effect at low magnetic fields, and the chemical potential could be extracted with Eq. (2). However, if puddles have formed, the correct carrier densities cannot be extracted with Eq. (1); to address this problem, we developed the following methodology.

III. THEORETICAL MODEL

Imagine that the system breaks into electron and hole puddles of size S_{n_i} and S_{p_i}. Inside each hole puddle with density p_i and n_i the following energy relation exists:

$$|V_g| = \frac{e(p_i - n_i) - Q_i^{ss}}{c_g} + \mu(p_i)/e + \phi(V_{FB_i}), \quad (3)$$

where we express the electrostatic energy as a plate capacitor, thanks to the thin oxide layer (<15 nm), which is smaller than a typical puddle size. Q_i^{ss} is the total immobile impurity charge density trapped at the graphene oxide interface, and $\phi(V_{FB})$ is the surface electric potential at the silicon-oxide interface. A similar expression exists for the electron puddles (with the exception of the signs), and after some algebra, one obtains the following relation:

$$-\left(V_g - V_d^p - V_d^n\right)$$
$$= \frac{S_p}{S_T}\frac{ep}{c_g} - \frac{S_n}{S_T}\frac{en}{c_g} + \frac{S_n}{S_T}V_d^p + \frac{S_p}{S_T}V_d^n + \mu(n,p)/e$$
$$+ \phi(V_{FB}), \quad (4)$$

where $S_p = \sum_i S_{p_i}$ ($S_n = \sum_i S_{n_i}$) is the total area of the hole (electron) puddles, $S_p p = \sum_i S_{p_i} p_i$ ($S_n n = \sum_i S_{n_i} n_i$), and $S_p Q_p^{ss} = \sum_i S_{p_i} Q_i^{ss}$ ($S_n Q_n^{ss} = \sum_i S_{n_i} Q_i^{ss}$). In addition, $Q_{p(n)}^{ss} = c_g V_d^{p(n)}$, $S_p + S_n = S_T$ is the total graphene area, and the total chemical potential of the inhomogeneous graphene is given by

$$\mu(n,p) = \sum_i S_{p_i}\mu(p_i) - \sum_i S_{n_i}\mu(n_i), \quad (5)$$

which can be approximated by

$$\mu_{\text{app}}(n,p) = \frac{S_p}{S_T}\mu(p) - \frac{S_n}{S_T}\mu(n), \quad (6)$$

as expected for a system with two noninteracting species.

In the limit of homogenous graphene, for example, p type, $S_n \to 0$, and Eq. (2) is restored. The carrier density is

measured by the Hall effect, and $\mu(p)$ is extracted. However, as the density decreases, puddles form, and the exact densities become unknown. In a recent paper, Li *et al.*[14] developed a theoretical model for transport in inhomogeneous graphene. They introduced a single parameter, s, which described the standard deviation of the electrostatic potential fluctuations of the graphene landscape with a Gaussian distribution. Consequently, the density of states of both the electrons and the holes becomes finite at the Dirac point, and electrical transport may prevail. This model also predicts the temperature dependence of the carrier densities, the chemical potential, and the total conductivity based on the effective-medium theory of conductance in composite mixtures.[15] Thus, incorporating the model of Li *et al.* with Eq. (4) and with our conductivity data, we can self-consistently solve this set of equations and extract the fluctuation parameter, s; the densities; and the chemical potential.

To be more specific, the electrostatic potential energy (V) distribution, $P(V)$, is given by[14]

$$P(V) = \frac{1}{\sqrt{2\pi s^2}}\exp(-V^2/2s^2), \quad (7)$$

and all others quantities, such as the DOS, the electron and hole densities, the conductivity, and the chemical potential, can be derived from this Gaussian distribution. The electron DOS is given by

$$D_e(E) = \int_{-\infty}^{E} \frac{g_s g_v(E_V)}{2\pi(\hbar v_F)^2} P(V) dV, \quad (8)$$

where g_s and g_v are the spin and valley degeneracies, and v_F is the graphene Fermi velocity. At the CNP, the densities of holes and electrons are equal and are given by

$$n_D(T) = p_D(T) = n_0\left(1 + \frac{\pi^2}{3}\left(\frac{k_B T}{s}\right)^2\right), \quad (9)$$

where $n_0 = s^2/2\pi/(\hbar v_F)^2$, $\hbar = h/2\pi$, and h is Planck constant. References 5 and 6 argue that the electron-electron interaction within the Hartree-Fock approximation renormalizes the Fermi velocity by $v_F \simeq v_0(1 + 0.25 r_s)$ (for $n = 10^{12}$ cm^{-2}), where $v_0 = 10^8$ cm/s, and $r_s = e^2/\hbar v_0\kappa$ is the graphene coupling constant. κ is the effective dielectric constant given by $\kappa = (1 + \kappa_{ox})/2$, where κ_{ox} is the dielectric constant of the oxide substrate underneath the graphene. For example, for devices on SiO$_2$ (HfO$_2$), $r_s = 0.89$ ($r_s = 0.27$), and electron-electron corrections are expected to play a minor role.[6] In Ref. 1, the authors estimated the correction to v_F from electron-electron interactions to be $\simeq 10\%$ for graphene on SiO$_2$, and the correction is expected to be much smaller for an HfO$_2$ gate oxide. In this study we have incorporated these corrections through the renormalization of v_F as well.

The hole DOS is $D_h(E) = D_e(-E)$, and the chemical potential, $\mu(n,p,T)$, is the solution of the following equation:

$$\int_{-\infty}^{E_F} D_e(E) dE - \int_{E_F}^{\infty} D_h(E) dE$$
$$= \int_{-\infty}^{\infty} \frac{D_e(E) dE}{1 + \exp[\beta(E - \mu)]} - \int_{-\infty}^{\infty} \frac{D_h(E) dE}{1 + \exp[\beta(\mu - E)]}, \quad (10)$$

where E_F is the chemical potential at $T = 0$, $\beta = 1/k_B T$, and k_B is the Boltzmann constant. Because the carrier densities and the chemical potential are solely functions of s, it is possible to solve Eqs. (4) and (10) self-consistently. However, the relation between the densities and the applied gate voltage is missing; specifically, the relation is missing in the inhomogeneous regime. To this end, we utilize the conductivity data that we measured and an effective-medium theory of conductance in composite mixtures;[15] this theory assumes the following relation for the total conductivity:

$$\sigma_t = \left(q - \frac{1}{2}\right)\left[(\sigma_1 - \sigma_2) + \sqrt{(\sigma_1 - \sigma_2)^2 + \frac{4\sigma_1\sigma_2}{(2q-1)^2}}\,\right],$$

(11)

where σ_1 (σ_2) is the electron (hole) conductivity, which includes both the Drude-like conductivity for each carrier type and the hole (electron) Boltzmann activation term over the electron (hole) puddles, and q is the fraction of the total area occupied by electrons. Solving Eqs. (4), (10), and (11) self-consistently with a single fitting parameter, s, we can extract the carrier densities, n and p, and the chemical potential of the system, μ, at the measured temperatures.

IV. RESULTS AND DISCUSSION

Figure 2 depicts the measured density as a function of the gate voltage for the SLG on 15 nm of HfO$_2$ (sample A). Near the CNP, the Hall voltage vanishes, and the calculated density diverges (black line). In addition, we plot n_H and p_H as extracted with Eq. (1). Initially, we assume that as long as these two values for the densities coincide, the system is homogenous; beyond the turning point, the system has broken into electron and hole puddles, and the effective-medium theory can be adopted. Because we know our dopant concentration and oxide thickness very accurately from time of flight (TOF-SIMS) and ellipsometry analyses, we have a
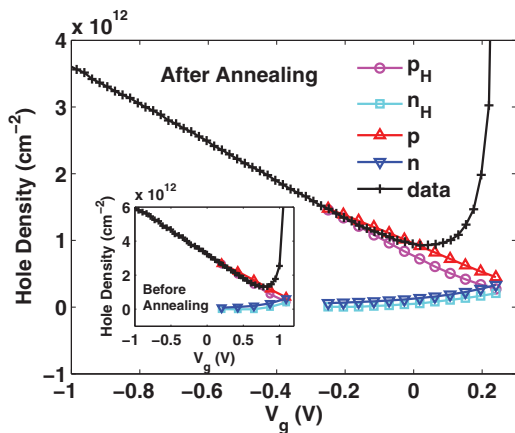

FIG. 2. (Color online) Measured and calculated hole densities as a function of the gate voltage at 300 K for SLG on 15 nm of HfO$_2$ before (inset) and after (main) annealing. The black line (cross) represents the measured data, the magenta and light blue lines (circle and square) are the calculated p_H and n_H from Eq. (1), and the red and blue lines (up and down triangles) are the corrected p and n densities extracted from the self-consistent procedure.
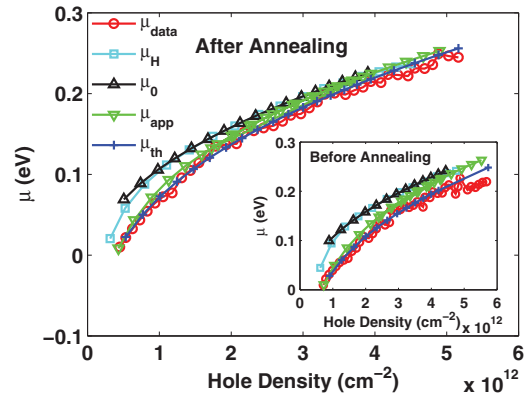

FIG. 3. (Color online) Chemical potential as a function of hole density before (inset) and after (main) annealing. The red line (circle) is the experimental data, the blue line (cross) is the theoretical fit of the self-consistent model, the black line (up triangle) is μ_0 for the unipolar system with a hole density of p_H [Eq. (12)], and the green and light blue lines (down triangle and square) are two approximations based on Eq. (6). The first approximation invokes the (p,n) couple, and the second approximations invokes (p_H, n_H), as discussed in the main text.

single fitting parameter, s, in our self-consistent procedure for the inhomogeneous region. The introduction of v_F as an additional fitting parameter did not change the results much, and through all our calculations, v_F was found to be $v_F = (1 \pm 0.05) \times 10^8$ cm/s. $V_d^{p(n)}$ were chosen to be equal to V_{Dirac}, which was extracted from the minimum of the conductance as a function of the gate voltage data. The results of this analysis are plotted in Fig. 3 before (inset) and after (main) annealing for the p-type branch. Similar results were found for the n-type branch as well. The red curve presents the experimental data derived from Eq. (4) at 300 K. The black curve depicts μ_0 as calculated from p_H alone. At $T = 0$, $\mu_0(p, T = 0) = \hbar v_F \sqrt{\pi p}$, which is simply the Fermi energy of the noninteracting electrons, and at finite T, μ_0 is the solution of the following equation:[16]

$$\frac{1}{2}\left(\frac{T_F}{T}\right)^2 = F_1(\beta\mu_0) - F_1(-\beta\mu_0),$$

(12)

where $T_F = E_F/k_B$, $F_1(x) = \int_0^\infty [1 + \exp(t - x)]^{-1} t\,dt$, and $t = E/k_B T$.

Because the chemical potential must be zero at the Dirac point, it is clear that $\mu_0(p, T)$ cannot be an adequate expression for the chemical potential in the vicinity of the CNP. The blue line presents the theoretical chemical potential according to the Gaussian disorder distribution, with a standard deviation $s = 125\,(93.5) \pm 2$ meV before (after) annealing, which was found self-consistently from Eqs. (4), (10), and (11). Based on the opposite signs of the chemical potential for each carrier type [Eq. (6)], two approximations can be tested. The first approximation is depicted in light blue (μ_H) in the inset of Fig. 3, and is described by $\mu(n_H, p_H) = [p_H\mu_0(p_H) - n_H\mu_0(n_H)]/(p_H + n_H)$. The second approximation, which is plotted with the green curve (μ_{app}), corresponds to the chemical potential given by the corrected carrier densities (solved self-consistently) but with the simple approximation of $\mu_{\text{app}}(n, p) = [S_p\mu_0(p) - S_n\mu_0(n)]/S_T$. As shown, the
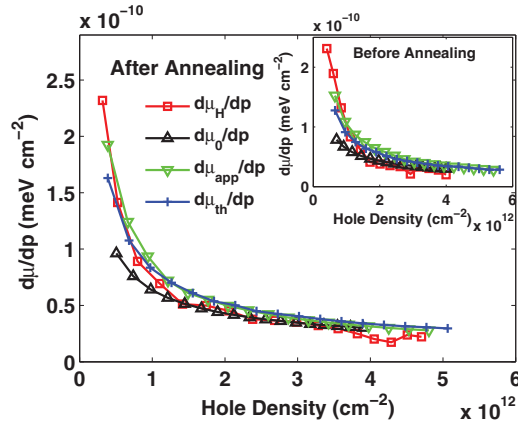
FIG. 4. (Color online) Inverse compressibility as a function of hole density. These plots were obtained from the numerical derivative of Fig. 3 with the same color codes (with the exception of the red) and symbol definitions.

agreement between theory (blue) and experiment (red) is very good, and as the density approaches the Dirac point, the disagreement between the previous models and the experiment increases. For the experimental data plotted in Fig. 3, the best fit was obtained for $s = 125\,(93.5) \pm 2$ meV before (after) annealing; this value corresponds to a strong disorder potential and translates to density fluctuations of $\delta p(\delta n) \approx 1$–$2 \times 10^{12}$ cm^{-2}. Consequently, we anticipate that electron and hole puddles will start to appear at higher hole densities than those predicted by the two-carrier Hall model.

For the data prior to annealing, the inset of Fig. 2 depicts, in addition to the experimental data, the corrected carrier densities (red and blue), which were found self-consistently, as opposed to the Hall densities which were based on Eq. (1) (magenta and light blue). Indeed, one finds that the deviation from the single-carrier phase (p type) occurs much before the turning point of the experimental data, and both the electron and hole densities are higher than those calculated with the two-carrier Hall model. This outcome becomes even more significant if the inverse compressibility ($K^{-1} = \partial\mu/\partial p$) of

inhomogeneous SLG is measured. The inset of Fig. 4 depicts such an analysis; for Fig. 3, instead of taking the derivative of the red line, which is too noisy, we took the derivative of the theoretical best-fitted curve of the red line (blue line). The color codes for the two figures are the same. From the inset of Fig. 4, it is evident that at high densities, in which the system has a single carrier type (holes), K^{-1} is approximately identical for the four models, but as the SLG becomes inhomogeneous and as the electron and hole puddles form, the measured inverse compressibility (blue line) deviates significantly from the other simplified models.

We performed the above analysis at different temperatures and were able to extract the temperature dependence of s, p, and n; the carrier mobility (μ_0); and the chemical potential (μ). Moreover, it has been shown in several studies that annealing in different environments may clean graphene flakes, reduce the disorder potential of the graphene, and increase its mobility.[12,13,17,18] Therefore, we annealed the previous sample in vacuum with high current at 300 K, and we repeated all of the above measurements over a temperature range of 1.7–300 K. From the transfer characteristics, two main features arose after annealing: (a) The Dirac point shifted towards the origin, as expected after the removal of charged impurities, and (b) the transfer characteristics became narrower. Indeed, the mobility increased approximately 2-fold from 2000 cm^2 V^{-1} s^{-1} to 4000 cm^2 V^{-1} s^{-1} at the high density of 5×10^{12} cm^{-2}. The same chemical potential analysis discussed previously was also performed for sample A after annealing, and the results for the chemical potential and the inverse compressibility at 300 K are plotted in the main panels of Figs. 3 and 4, respectively. The raw data for the Hall density and the corrected p and n densities in the inhomogeneous region are depicted in the main panel of Fig. 2. As expected, after annealing, the formation of puddles begins at lower densities; however, puddle formation still begins before the turning point of the Hall data, and the deviation from μ_0 and $K_0^{-1} = \partial\mu_0/\partial p$ becomes significant at low densities.

A comparison of the two sets of data reveals that the Dirac point or the CNP shifts with temperature for both measurements, as shown in Fig. 5(a). Moreover, the
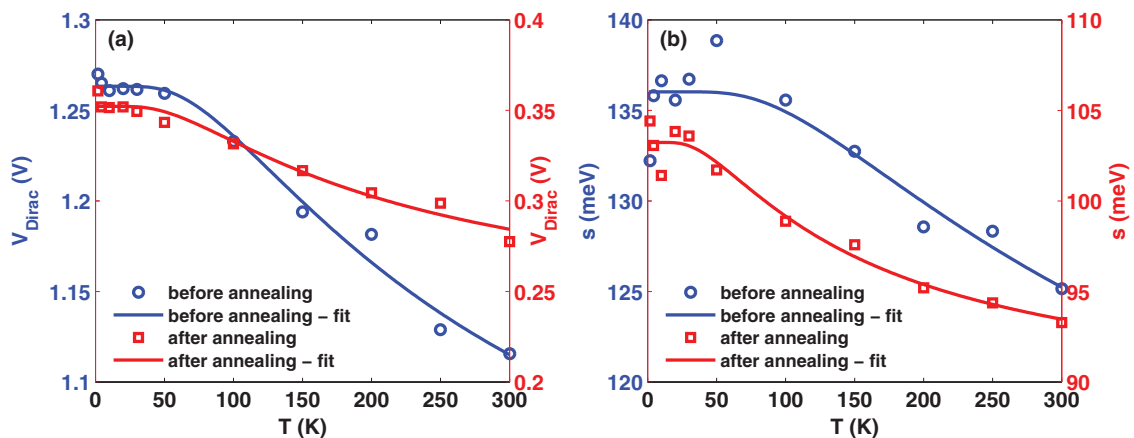

FIG. 5. (Color online) (a) Measured V_{Dirac} as a function of T for SLG on 15 nm of HfO$_2$ (sample A) before (blue circles) and after (red squares) annealing. Similarly, the blue and red lines are the best fits for activation-type behavior. (b) Calculated s from the self-consistent procedure as a function of T for sample A before (blue circles) and after (red squares) annealing. Similarly, the blue and red lines are the best fits for activation-type behavior.
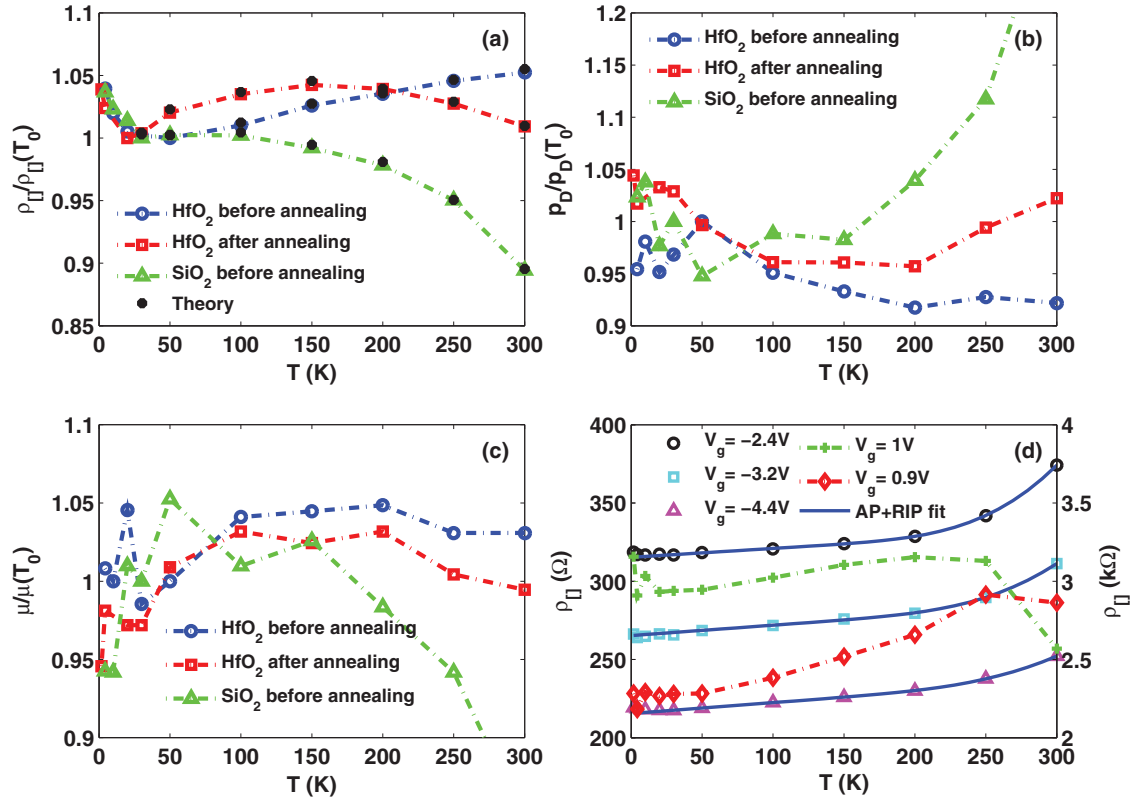
FIG. 6. (Color online) (a) Measured relative sheet resistance $[\rho(T)/\rho(T_0)]$ at the CNP, (b) relative hole density at the CNP $[p_H(T)/p_H(T_0)]$, and (c) relative mobility $[\mu(T)/\mu(T_0)]$ as a function of T for sample A before and after annealing and sample B. (d) Sheet resistance of sample B as a function of temperature for different SLG densities from high densities (pink triangles, light blue squares, and black circles—left axis) to those near the Dirac point (red diamonds and green crosses—right axis). The blue lines are the best fits to the experimental data with Eq. (13), in which acoustical phonons (AP) and ripples from the substrate (RIP) are the dominant source for the temperature dependence of sheet resistance.

experimental data can be fitted very well to the following equation: $V_{Dirac}(T) = V_{Dirac}(T = 0) - V_0 \exp(-\Delta/T)$, and Δ is $\sim$253 K (188 K) before (after) annealing. We argue that Δ plays the role of an activation energy for the charged impurities, and consequently, the CNP shows this T dependence. Because in both cases, the CNP is positive and shifts towards the origin as T increases, the surface states lose electrons to the graphene and the disorder potential is altered. Figure 5(b) depicts the standard deviation, s, of the disorder potential as a function of T, as found using the self-consistent model, and two main results can be observed. First, after annealing, s is indeed smaller by almost 30% compared with the same device before annealing. Second, in both cases, s decreases as T increases, and s is well fitted by activation-type behavior [similar to that observed for $V_{Dirac}(T)$] with $\Delta \approx 265$ K (135 K) before (after) annealing. Although the activation energies for V_{Dirac} and s are somewhat different after annealing, one should bear in mind that V_{Dirac} monitors the mean of the disorder potential distribution and that s^2 reflects the variance of this distribution; a more complex theory is required to quantitatively couple these two parameters. Nevertheless, because s affects the free carrier charge density near the CNP through the effective DOS [see Eq. (9)], we anticipate that the change of s with T will modify the graphene conductivity in the regime of the electron hole puddles as

well. Similar results were found for other SLG devices on 15 nm of HfO_2 and on 10 nm of SiO_2, with a mobility range between 1000 and 15 000 cm^2 V^{-1} s^{-1}. Figures 6(a) and 6(b) depict the relative sheet resistance $[\rho_\square(T)/\rho_\square(T = 30)$ K] and the relative hole density at the Dirac point $[p_D(T)/p_D(T = 50$ K)], respectively, as a function of T for sample A before and after annealing and for sample B, which is comprised of SLG on 10 nm of SiO_2. The circles, squares, and triangles in Fig. 6(a) show the measured sheet resistances at the CNP, and the black asterisks show the sheet resistances calculated with our self-consistent model; excellent agreement was achieved. Below 30 K, weak localization effects take place.[19] However, above 30 K, we observed nonmonotonic behavior for the sheet resistance as a function of temperature; this behavior is intriguing.

The temperature dependence of the conductivity of graphene has stimulated many theoretical and experimental studies.[16,20–24] Usually, this T dependence is weak from cryogenic temperatures upto 300 K because of poor electron-phonon coupling and because of the high energy of the optical phonons (0.2 eV). Because most studies have been performed on SiO_2, it is now believed that acoustical phonons contribute a linear T dependence to the resistivity, and that activation-type behavior arises from remote interfacial phonon (RIP) scattering by the polar optical phonons of

the substrates.[21,22,25] Other possibilities for the temperature dependance of the resistivity are based on the reduction of the screening efficiency of SLG as T increases. Recently, theoretical and experimental studies[14,26] raised and confirmed the possibility of nonmonotonic dependence $\rho(T)$ for a chemical vapor deposition (CVD) graphene based device, in which the mobilities are lower than those obtained by the exfoliation technique. The measured behavior was explained by the competition between two opposing processes: (a) the thermal activation behavior of carriers above the potential barriers within the puddle regime, which results in "insulating like" behavior at low temperatures, and (b) phonon scattering and a reduction in the screening of remote charged impurities as T increases, which are processes that yield "metallic like" behavior.

Our data, depicted in Fig. 6(a), exhibit nonmonotonic behavior in the opposite order. For sample A, before annealing, and for $T > 30$ K, the resistance increases as T increases to 300 K, although the curvature is negative; this curvature means that the sample is almost saturated and that insulating behavior at higher temperatures is possible. However, sample A after annealing and sample B show an increase in the sheet resistance as T increases, i.e., "metallic like" behavior, but as T increases further, both samples exhibit "insulating" type characteristics. Because we extracted the correct p and n densities in the inhomogeneous regime, as described previously, and because the total sheet resistance at the CNP has been measured, we can extract the mobilities of electrons and holes at the Dirac point (assuming $\mu_n = \mu_p = \mu_0$) and identify the origin of this nonmonotonic temperature dependence. Figures 6(a)–6(c) present three graphs of the temperature dependence of the sheet resistance at the Dirac point $\rho_\square(T)/\rho_\square(T_0)$ [Fig. 6(a)], the density, $p_D(T)/p_D(T_0)$ [Fig. 6(b)], and the mobility, $\mu_D(T)/\mu_D(T_0)$ [Fig. 6(c)], for samples A and B. Different T_0 values were used to avoid the influence of the weak localization correction in the current analysis. The three cases (sample A before and after annealing and sample B) exhibit an increase in mobility at low T ("insulating" behavior) and a decrease in μ at high T ("metallic" behavior); these behaviors qualitatively correspond well to the arguments discussed in Refs. 14 and 26. However, because s decreases for both samples as T increases, the densities at the CNP are influenced as well. For sample A before annealing, the decrease in s was not saturated at 300 K [see Fig. 5(b)], and as a result, the decrease in p_D as T was increased enforced "metallic like" behavior over the entire temperature range. However, for sample A after annealing and for sample B, the reduction of s as T was increased became saturated more quickly, and thermal activation of carriers at the CNP became more significant than the reduction of μ as T increased; this change resulted in the observed nonmonotonic temperature dependence.

This non metallic behavior is not restricted to the Dirac point only; it occurs near the Dirac point, where the system is strongly affected by the effective DOS. However, far from the Dirac point, where the system is homogenous, we do not expect to observe such a non monotonic temperature dependence. Figure 6(d) depicts $\rho_\square(T)$ of sample B at five densities; three that are far from the CNP (high densities), and two that are close to but not at the Dirac point (low

densities). For the high-density data, we followed the same analysis as Chen et al.[22] and found an excellent fit (blue lines) that consists of two contributions. The first contribution has a linear T dependence, and arises from acoustic phonons in SLG. The second contribution contains an activation energy term, which arises from ripples that originate from the SiO_2 substrate beneath the SLG. The best fit was obtained with the following equation:

$$\rho_\square(T) = \rho_0 + cD_A^2 T + \frac{a_1}{e^{(155\ \text{meV})/k_B T} - 1}, \qquad (13)$$

with two fitting parameters, D_A, which is the acoustic deformation potential, and a_1. c is a known constant, which contains the Fermi velocity, the speed of sound, and the mass density of graphene.[22] From our data, D_A was found to be 16 ± 1 eV, which is in good agreement with previous theoretical and experimental results,[20,22,27–29] and the RIP energy was $\hbar\omega = 155 \pm 10$ meV, as expected. However, no use was found for the lower surface optical phonon mode of $\hbar\omega = 59$ meV. At the two lower densities, such a fit does not hold; the nonmonotonic behavior resembles the same dependence as was found previously at the Dirac point [Fig. 6(a)] and arises from the same physical origin.

Finally, we would like to estimate the concentration of the impurities, n_i, the distance of the impurities from the SLG samples, d, and the effective dielectric constant, κ, for each sample and substrate. To that end, we utilize the self-consistent theory for graphene transport developed by Adam et al.[30] From the sheet resistance, the mobility near the Dirac point, and the exact densities at the CNP, the three unknown variables, n_i, d, and κ, are found numerically from the following set of equations:

$$\left(\rho_\square^{\text{max}}\right)^{-1} = \frac{e^2}{h} \frac{n^\star}{n_i} \frac{2}{G(2r_s)},$$
$$\frac{n^\star}{n_i} = 2r_s^2 C_0^{\text{RPA}}(r_s, a = 4d\sqrt{\pi n^\star}), \qquad (14)$$
$$\mu = \frac{2e}{h} \frac{1}{n_i G(2r_s)},$$

where $n^\star$ is the residual doping, and $G(x)$ and $C_0^{\text{RPA}}(r_s, a)$ are defined as in Ref. 30. For example, for sample A before (after) annealing at low T where Eqs. (14) are valid, one finds that $n_i = 5.3 \times 10^{12}$ cm^{-2} ($n_i = 2.5 \times 10^{12}$ cm^{-2}), $d = 0.4$ nm ($d = 0.5$) nm, and $\kappa = 7.1$ (7); these results are in good agreement with $\kappa = 6.3$, which is the expected dielectric constant of SLG located on top of a thin layer of PMMA (≈ 1 nm) with 15 nm of HfO_2 underneath. For sample B one finds that $n_i = 1.3 \times 10^{12}$ cm^{-2}, $d = 0.5$ nm, and $\kappa = 2.8$. This result is in good agreement with $\kappa = 2.4$ expected for sample B on top of thin layer of SiO_2.

V. CONCLUSIONS

In conclusion, we measure the chemical potential of SLG and observe that at low densities, where electron and hole puddles coexist, the chemical potential and the inverse compressibility are modified by the electrostatic disorder potential, which is described well by a Gaussian disorder distribution. In addition, nonmonotonic sheet resistance was observed and

was primarily attributed to the temperature dependence of the disorder potential itself. By extracting the electron and hole densities, one can describe the T dependence of the mobility from the overall $\rho(T)$ and can accurately study the temperature dependence of the different scattering mechanisms that affect the resistivity of graphene.

[1] J. Martin, N. Akerman, G. Ulbricht, T. Lohmann, J. H. Smet, K. Von Klitzing, and A. Yacoby, Nat. Phys. **4**, 144 (2008).

[2] L. A. Ponomarenko, R. Yang, R. V. Gorbachev, P. Blake, A. S. Mayorov, K. S. Novoselov, M. I. Katsnelson, and A. K. Geim, Phys. Rev. Lett. **105**, 136801 (2010).

[3] E. A. Henriksen and J. P. Eisenstein, Phys. Rev. B **82**, 041412 (2010).

[4] A. F. Young, C. R. Dean, I. Meric, S. Sorgenfrei, H. Ren, K. Watanabe, T. Taniguchi, J. Hone, K. L. Shepard, and P. Kim, Phys. Rev. B **85**, 235458 (2012).

[5] E. H. Hwang, Ben Yu-Kuang Hu, and S. Das Sarma, Phys. Rev. Lett. **99**, 226801 (2007).

[6] Q. Li, E. H. Hwang, and S. Das Sarma, Phys. Rev. B **84**, 235407 (2011).

[7] D. S. L. Abergel, E. H. Hwang, and S. Das Sarma, Phys. Rev. B **83**, 085429 (2011).

[8] K. S. Novoselov, A. K. Geim, S. V. Morozov, D. Jiang, Y. Zhang, S. V. Dubonos, I. V. Grigorieva, and A. A. Firsov, Science **306**, 666 (2004).

[9] E. M. Hajaj, O. Shtempluk, A. Razin, V. Kochetkov, and E. Y. Yaish (unpublished).

[10] See Supplemental Material at http://link.aps.org/supplemental/10.1103/PhysRevB.88.045128 for transconductance analysis.

[11] H. Xu, Z. Zhang, H. Xu, Z. Wang, S. Wang, and L.-M. Peng, ACS Nano **5**, 5031 (2011).

[12] J. Moser, A. Barreiro, and A. Bachtold, App. Phys. Lett. **91**, 163513 (2007).

[13] M. Ishigami, J. H. Chen, W. G. Cullen, M. S. Fuhrer, and E. D. Williams, Nano Lett. **7**, 1643 (2007).

[14] Q. Li, E. H. Hwang, and S. Das Sarma, Phys. Rev. B **84**, 115442 (2011).

[15] S. Kirkpatrick, Rev. Mod. Phys. **45**, 574 (1973).

[16] E. H. Hwang and S. Das Sarma, Phys. Rev. B **79**, 165404 (2009).

[17] K. I. Bolotin, K. J. Sikes, Z. Jiang, M. Klima, G. Fudenberg, J. Hone, P. Kim, and H. L. Stormer, Solid State Commun. **146**, 351 (2008).

[18] C. Chen, S. Rosenblatt, K. I. Bolotin, W. Kalb, P. Kim, I. Kymissis, H. L. Stormer, T. F. Heinz, and J. Hone, Nat. Nanotechnol. **4**, 861 (2009).

[19] F. V. Tikhonenko, D. W. Horsell, R. V. Gorbachev, and A. K. Savchenko, Phys. Rev. Lett. **100**, 056802 (2008).

[20] E. H. Hwang and S. Das Sarma, Phys. Rev. B **77**, 115449 (2008).

[21] S. Fratini and F. Guinea, Phys. Rev. B **77**, 195415 (2008).

[22] J.-H. Chen, C. Jang, S. Xiao, M. Ishigami, and M. S. Fuhrer, Nat. Nanotechnol. **3**, 206 (2008).

[23] S. V. Morozov, K. S. Novoselov, M. I. Katsnelson, F. Schedin, D. C. Elias, J. A. Jaszczak, and A. K. Geim, Phys. Rev. Lett. **100**, 016602 (2008).

[24] K. I. Bolotin, K. J. Sikes, J. Hone, H. L. Stormer, and P. Kim, Phys. Rev. Lett. **101**, 096802 (2008).

[25] K. Hess and P. Vogl, Solid State Commun. **30**, 807 (1979).

[26] J. Heo, H. J. Chung, S.-H. Lee, H. Yang, D. H. Seo, J. K. Shin, U-In Chung, S. Seo, E. H. Hwang, and S. Das Sarma, Phys. Rev. B **84**, 035421 (2011).

[27] S. Ono and K. Sugihara, J. Phys. Soc. Jpn. **21**, 861 (1966).

[28] V. Perebeinos, J. Tersoff, and P. Avouris, Phys. Rev. Lett. **94**, 086802 (2005).

[29] X. J. Zhou, J. Y. Park, S. M. Huang, J. Liu, and P. L. McEuen, Phys. Rev. Lett. **95**, 146805 (2005).

[30] S. Adam, E. H. Hwang, V. M. Galitski, and S. Das Sarma, Proc. Natl Acad. Sci. USA **104**, 18392 (2007).